



# Effect of urban function and landscape structure on the urban heat island phenomenon in Beijing, China

Lei Yao<sup>1</sup> · Ying Xu<sup>2</sup> · Baolei Zhang<sup>1</sup>

Received: 26 April 2019 / Revised: 19 June 2019 / Accepted: 20 June 2019 / Published online: 16 July 2019  
© International Consortium of Landscape and Ecological Engineering 2019

## Abstract

Rapid urbanization has aggravated the urban thermal risk and highlighted the urban heat island (UHI) effect. To improve understanding on the effect of urbanization on the UHI effect, it is essential to determine the relationship between the UHI effect and the complexities of urban function and landscape structure. For this purpose, 5116 urban function zones (UFZs), representing the basic function units of urban planning, were identified in Beijing. Land cover and land surface temperature (LST) values were extracted based on remote sensing data. UFZ, land cover, and LST were used to represent the urban function, landscape, and UHI characteristics, respectively. Then, the effects of urban function and landscape structure on the UHI effect were examined. The results indicated that the urban thermal environment exhibited obvious spatiotemporal heterogeneity due to the variation of urban function and landscape complexity: (1) UFZs showed significantly different LST characteristics for different functions and seasons, and the mean LST gap among different types of UFZ can reach 1.72–3.85 °C. (2) During warm seasons, the UHI region is mainly composed of residential, industrial, and commercial zones, while recreational zones contribute as an important UHI source region during cold seasons. (3) Urban developed land and forest are the most important landscape factors contributing to the UFZ effect in the urban thermal environment. These findings have useful implications for urban landscape zoning to mitigate the UHI effect.

**Keywords** Urban heat island · Land surface temperature · Urban function zone · Urban landscape · Urban planning

## Introduction

The urban heat island (UHI) phenomenon, which is one of the most concerning urban environmental issues, has become increasingly important along with the urbanization process, which has changed the surface energy balance by replacing natural land with impervious urban land (Gago et al. 2013; Haashemi et al. 2016). Additionally, increasing anthropogenic activities in urban areas, such as vehicle traffic, air conditioning, and emissions from factories, also

increase the urban thermal burden (Carlson and Traci Arthur 2000). The growing UHI effect may lead to several adverse effects, such as increased thermal discomfort and energy consumption (Almusaed 2011), air pollution (Vos et al. 2013), wastage of water resources (Yang et al. 2012), and damage to human health and the balance of the local ecosystem (Gago et al. 2013). These negative effects of the UHI phenomenon pose significant threats to sustainable development of urban ecosystems, and have thus drawn greater attention from urban planners and the research community.

To better understand and solve the problem of the UHI effect, it is essential to establish its relationship with urban spatial structure (Li et al. 2011; Peng et al. 2016). As stated by Zhou et al. (2014), the UHI effect includes both air temperature and land surface temperature (LST) components. Urban air temperature was initially adopted as an effective indicator of urban surface energy characteristics to quantify the UHI phenomenon in urban thermal studies (Arnfield 2003; Taha 1997). However, air temperature measurements in UHIs are restricted to a limited number of climate stations, which may prevent the establishment

✉ Lei Yao  
alex\_yaolei@126.com

✉ Baolei Zhang  
blzhangsd@163.com

Ying Xu  
xuy\_1986@126.com

<sup>1</sup> College of Geography and Environment, Shandong Normal University, Jinan 250014, China

<sup>2</sup> School of Civil Engineering, Shandong Jiaotong University, Jinan 250023, China

of a relationship between the air temperature and urban spatial characteristics (Arnfield 2003). In addition, the air temperature in urban areas generally shows greater spatiotemporal variation compared with the LST (Chen et al. 2014, 2016). LST values derived from remote-sensing data, by contrast, have higher, continuous spatial coverage and can be closely related to landscape modifications due to urbanization (Amanollahi et al. 2016; Chen et al. 2016). In addition, LST values show strong correlation with near-surface air temperatures (Sun et al. 2013; Weng 2009). Therefore, remotely sensed LST values have often been used to indicate the urban thermal environment.

A considerable amount of studies have been conducted to assess the relationship between LST and urban land surface characteristics (Li et al. 2011; Peng et al. 2016; Zhou et al. 2011), enabling the classification of urban landscapes (i.e., land use/cover) as heating and cooling surfaces according to their thermal features. Generally, heating surfaces, which would aggravate the UHI effect, are considered to include artificial surfaces such as building roofs and paved roads, while cooling surfaces (which will alleviate the UHI effect) are associated with some types of open urban spaces and water bodies (Cao et al. 2010; Gago et al. 2013; Kardinal Jusuf et al. 2007). Thus, the proportions of these urban landscape types have an essential impact on the spatiotemporal variations of the LST (Dos Santos et al. 2017). Urban landscape planning can be implemented to benefit urban thermal comfort, requiring the rearrangement of not only the urban spatial landscape (Kardinal Jusuf et al. 2007) but also urban functions, which are directly related to urban socioeconomic and anthropogenic activities (Sun et al. 2013). However, few studies have tried to investigate the interactions between the UHI effect and urban functions (Li et al. 2011; Peng et al. 2016; Zhou et al. 2011). According to Tian et al. (2010) and Sun et al. (2013), urban function zones (UFZs) can be used to define regions with specific socioeconomic functions, having similar spatial characteristics, anthropogenic activity, and energy consumption. In addition, the spatial boundary of UFZs is usually formed by urban streets, which act as thermal barriers. These factors mean that each type of UFZ has a unique outdoor thermal characteristic. Using UFZs as the unit to study the UHI effect thus enables better conclusions to be drawn regarding urban planning to improve the urban thermal environment.

In this study, the core region of Beijing was selected as a case study area to investigate the variations of the UHI effect from the perspective of UFZs and the landscape structure. The specific aims of this study are: (1) to explore the spatiotemporal heterogeneity of the LST for different types of UFZ and seasons and (2) to quantify the effects of the landscape composition on the UHI effect, followed

by a discussion on the potential implications for urban management.

## Methodology

### Study area

As the capital city of China, the Metropolitan Region of Beijing (39°26′–41°03′N, 115°25′–117°30′E.) covers an area of approximately 16,800 km<sup>2</sup>, comprising 16 districts, with a population of nearly 20 million in 2011 (Beijing Statistical Bureau 2012). The city, having a typical continental monsoon climate, has an average temperature of 12 °C and distinct seasons. Since the late 1980s, Beijing has undergone a remarkable urbanization process. Owing to this rapid urban expansion, UHI effects in Beijing have become increasingly significant (Sun and Chen 2012), being further aggravated by urban environmental conditions, such as the local climate and air quality (Kardinal Jusuf et al. 2007; Ma et al. 2010). The area examined in this study is a highly urbanized region within the fifth ring road of Beijing, covering an area of nearly 667 km<sup>2</sup> (Fig. 1).

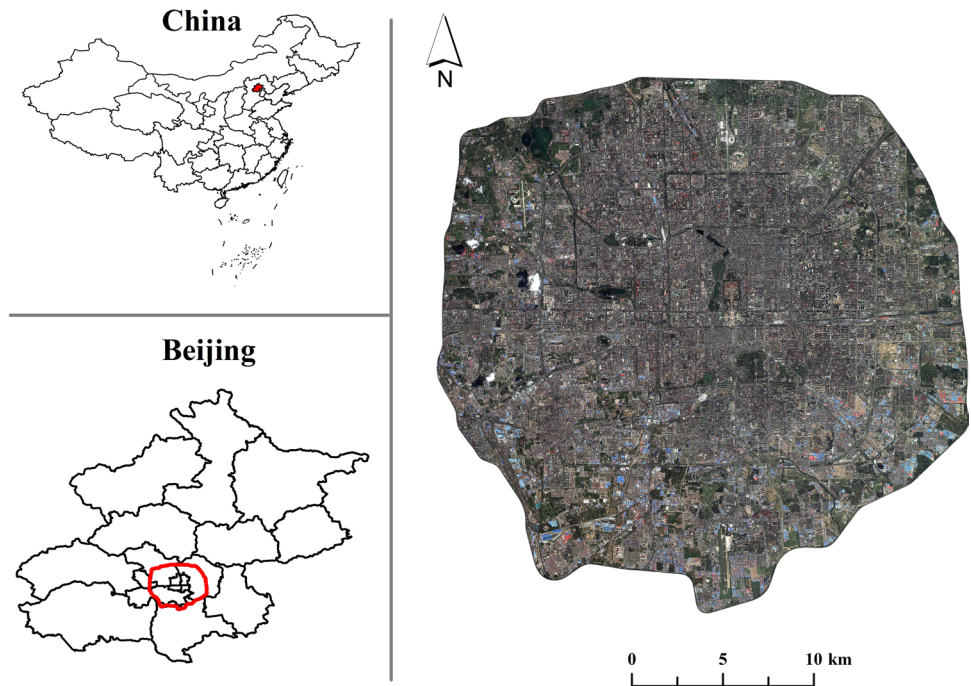
### Data preparation

The data was mainly obtained from remote sensing, including IKONOS and Landsat 8 images. The IKONOS image contained four bands (three visible and one near infrared) with spatial resolution of 4 m, and one panchromatic band with spatial resolution of 1 m. The Landsat 8 images consisted of eight bands (visible, near infrared, and shortwave infrared) with spatial resolution of 30 m, one panchromatic band with spatial resolution of 15 m, and two thermal infrared bands with spatial resolution of 100 m. All the satellite images were rectified and georeferenced to a common universal transverse Mercator (UTM) map base using a first-order polynomial transformation.

### Land cover and UFZ identifications

The IKONOS image was first applied to extract the land cover types in the study area (<https://www.satimagingcorp.com/satellite-sensors/ikonos/>). The image was captured in summer (29 July 2012) to provide detailed information on vegetation. Prior to classification, the spectral bands were pan-sharpened to the panchromatic image for higher spatial resolution (1 m). Six types of land cover (i.e., developed land, water body, farmland, tree canopy, lawn, and bare land) were extracted from the IKONOS image by adopting an object-based classification approach (Yao et al. 2015; Zhou and Cadenasso 2012). The remote-sensing image was first segmented into several “objects”

**Fig. 1** Spatial location of the study area



by grouping neighboring pixels with similar feature values (i.e., spatial, textural, spectral, color, and band ratio). Then, multiple rule sets were established to classify these “objects” as belonging to different land cover categories. Finally, we merged the geo-body shadows into actual cover types manually. Thereafter, ground-truthing analysis was conducted by verifying nearly 400 random points after classification. The overall accuracy of the classification

was 85.8% with kappa coefficient of 0.75. The classification result is shown in Fig. 2.

The IKONOS image was then used to retrieve detailed information on the UFZs. Sun et al. (2013) suggested that urban road networks serve as barriers that may possibly cut off thermal advection at a local scale. Thus, the geographic boundaries of each UFZ were mainly defined using linear landscape elements in urban regions, such as urban roads

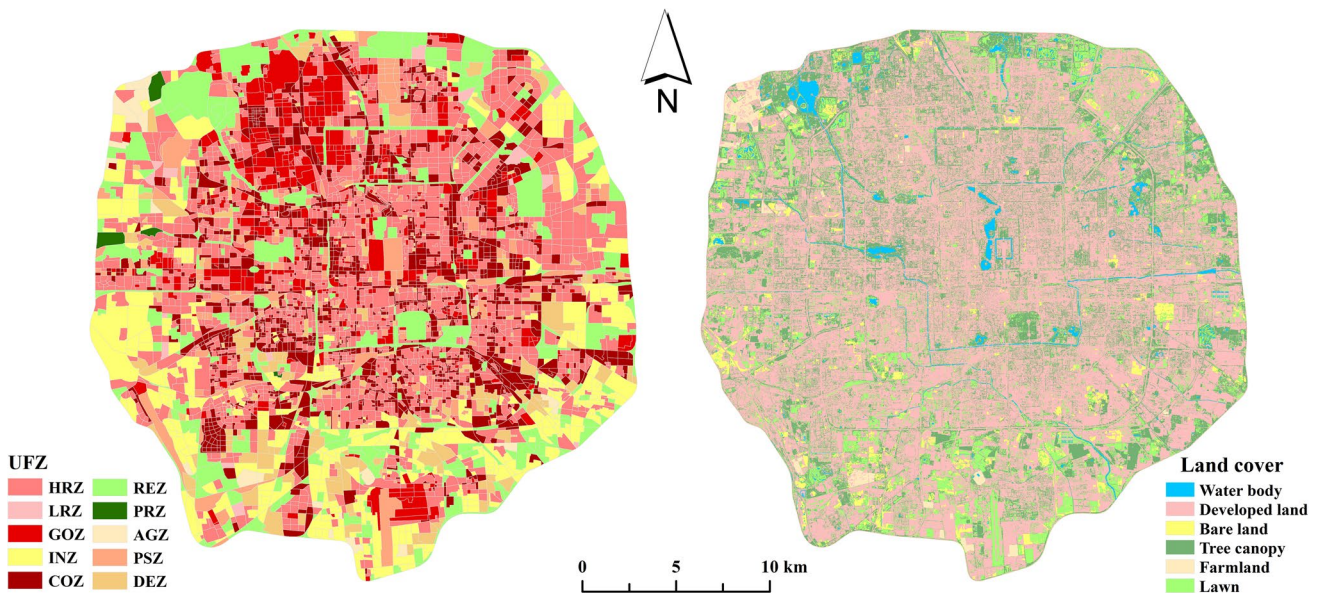


**Fig. 2** Land cover and urban function zone of the study area

and canal networks. Following the detailed procedure provided by Sun et al. (2013) and Yao et al. (2015), we manually delineated the entire study area into a total of 5116 UFZs according to the IKONOS image. Then, ten types of UFZ were categorized (Table 1; Fig. 2), including high-density residential zone (HRZ), low-density residential zone (LRZ), government zone (GOZ), industry zone (INZ), commercial zone (COZ), recreational zone (REZ), preservation zone (PRZ), agricultural zone (AGZ), public service zone (PSZ), and development zone (DEZ). The detailed urban functional information for each type of UFZ was verified based on internet query (e.g., Google Maps) and field investigation.

### Land surface temperature extraction

The thermal infrared bands (band 10, 10.6–11.2  $\mu\text{m}$ ) of the Landsat 8 images were used to retrieve the LST data in the study area. To explore the LST variations for different UFZs at the annual scale, Landsat images were acquired between the years of 2014 and 2015, covering each season, on 15 May 2014 (average air temperature 21.8  $^{\circ}\text{C}$ ), 19 August 2014 (25.8  $^{\circ}\text{C}$ ), 6 October 2014 (14.2  $^{\circ}\text{C}$ ), 25 December 2014 (−0.7  $^{\circ}\text{C}$ ), and 15 March 2015 (9.8  $^{\circ}\text{C}$ ). Each image was cloud free with highly clear atmospheric condition. The thermal infrared bands were resampled at spatial resolution of 30 m to facilitate the subsequent LST calculation. LST values were extracted by following the detailed algorithm provided by Chen et al. (2016) and Zhou et al. (2014). First, the pixel digital number (DN) values of the Landsat images were calibrated to top-of-atmospheric (TOA) radiance ( $L_{\lambda}$ ) based on the conversion algorithm provided by United States Geological Survey (USGS). Then, the land surface emissivity ( $\epsilon$ ) was estimated based on the land cover maps; The  $L_{\lambda}$  was then converted into surface-leaving radiance, corrected

using the emissivity value of each land cover type. Finally, LST values (in units of  $^{\circ}\text{C}$ ) were derived using the Landsat specific estimate of the Planck curve (Chen et al. 2016; Zhou et al. 2014). The generated image layers of the LST are shown in Fig. 3.

### Data analysis

The details of the landscape structure and LST were both summarized in each UFZ patch by overlapping the geographical information system (GIS) layer of the UFZs and the raster images of the land cover and LST (Fig. 4). The mean LST values were then used as the key variable in later analysis, to indicate the thermal characteristics of the UFZs in different seasons (Sun et al. 2013; Zhou et al. 2011).

A spatial clustering tool (Anselin Local Moran's I) was adopted to analyze all five periods of LST data, in order to explore the land surface thermal variations in the study area. This is one of the most standard tools to characterize the local spatial autocorrelation condition of a set of weighted features (with various values and spatial locations), showing the similarity of a location to its neighbors, and tests the significance of its similarity (Anselin 1995; Mitchell 1999). This method can be used to identify significant clusters of high or low values (i.e., hot and cold spots) (Meng 2016). Details of the theory of Anselin Local Moran's I and its algorithm can be found in Mitchell (1999). The output of this tool can be mapped to distinguish between statistically significant ( $p < 0.05$ ) clusters of high values (HH) and low values (LL), as well as outliers with high value (HL) and low value (LH). The HH and LL clusters are considered to represent hot and cold spots, respectively.

All the generated GIS layers of the LST were imported into ArcGIS software (version 10.3). The key parameters

**Table 1** Details of urban function zones (UFZs) in the study area

UFZ	Description
High-density residential zone (HRZ)	Services for citizens; typical residential communities in Beijing, including low- and high-rise buildings with dense population
Low-density residential zone (LRZ)	Services for citizens; lower impervious fraction; mainly low-rise buildings with sparse population
Government zone (GOZ)	Services for civil servants and students; government buildings, public organizations, research institutes, and campuses
Industry zone (INZ)	Services for production workers and laborers; city infrastructure and industrial factories, energy, and supply of resources
Commercial zone (COZ)	Services for business and commercial workers; city malls, retail businesses, and public amenities such as restaurants, hotels, etc.
Recreational zone (REZ)	Services for tourists and residents; urban parks, golf courses, and scenic areas with relatively high green coverage
Preservation zone (PRZ)	Services for tourists and residents; open space with natural and artificial green space such as forest parks
Agricultural zone (AGZ)	Services for agricultural workers; cultivated land, greenhouses, and orchards
Public service zone (PSZ)	Services for citizens, such as hospitals, libraries, museums, stadiums, and city squares
Development zone (DEZ)	Services mainly for construction workers; undeveloped open space and demolition areas

**Fig. 3** Land surface temperature (LST, unit in °C) of the study area

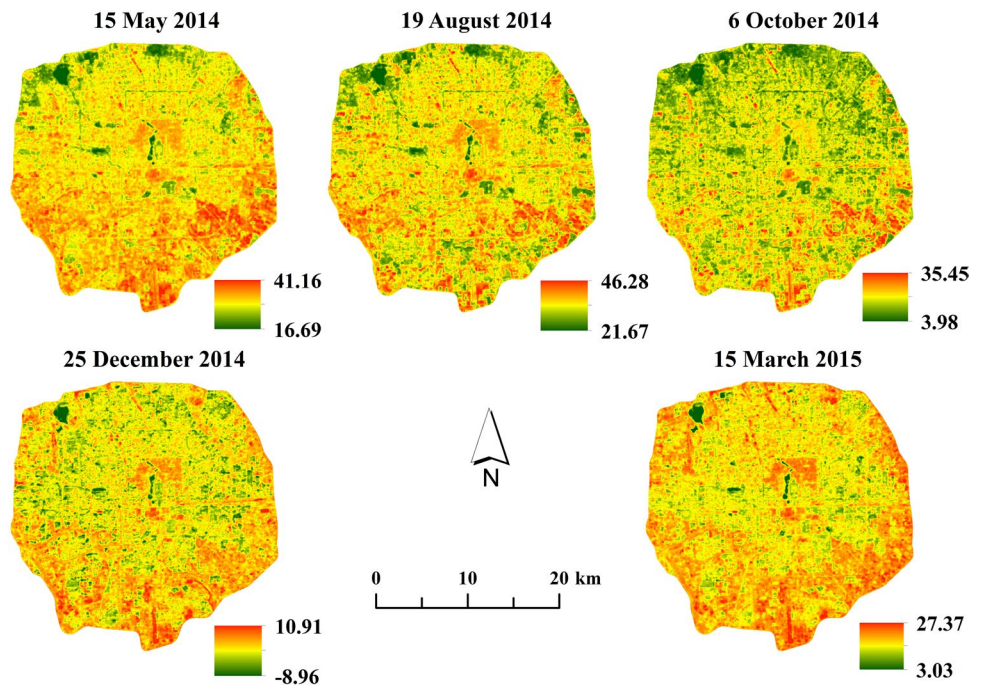
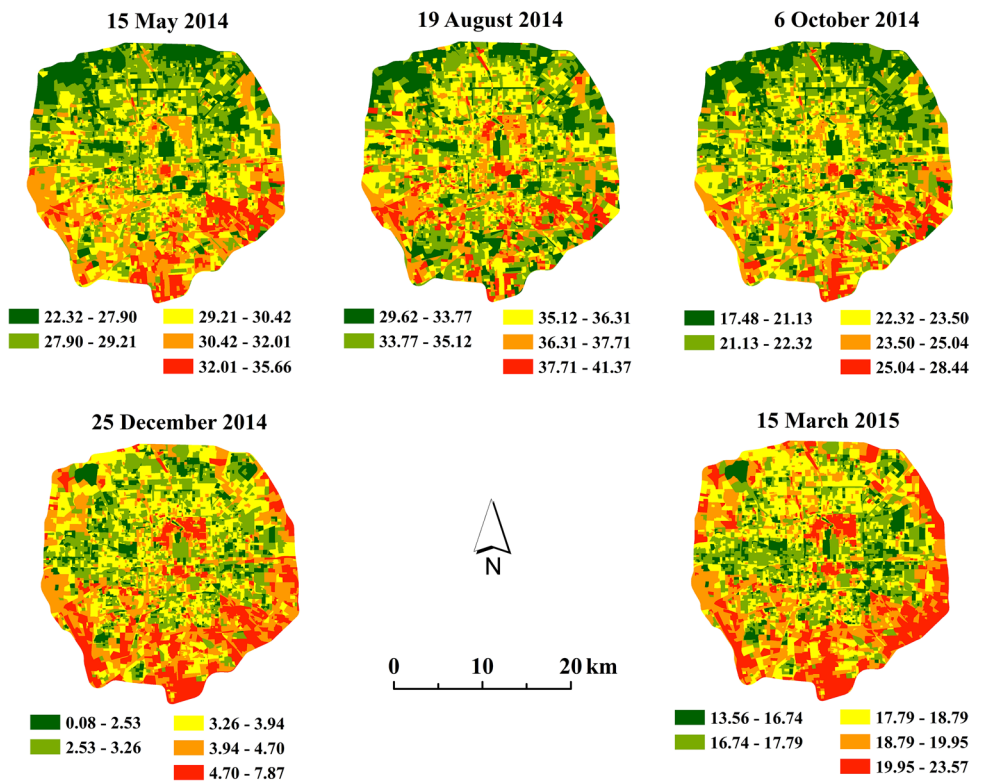


**Fig. 4** Mean values of land surface temperature (LST, unit in °C) of urban function zones. \*Jenks Natural Breaks for the class ranges



for this tool, including the input feature, conceptualization of spatial relationships, and distance method, were set as the mean LST values of the UFZs, the inverse distance (assuming that nearby neighboring features have a greater influence on the computations for a target feature than features that are far away), and Euclidean distance,

respectively, while the other parameters were set as default.

Based on the spatial clustering results, Pearson correlation analysis was applied to examine the potential relationship between the LST characteristics and land cover structures of UFZs in HH and LL clusters, respectively (Zhou

et al. 2011). Then, the main land cover factors responsible for the LST variations in different seasons were selected and discussed for future urban landscape planning.

ENVI software (version 5.1) was adopted for land cover identification and LST extraction, ArcGIS (version 10.3) was used for UFZ delineation and spatial analysis, and statistical analysis was accomplished by using SPSS (version 22).

## Results

### Spatial details of UFZs

The spatial analysis revealed that HRZ occupied the largest part of the study area (21254.39 ha), followed by COZ (10189.22 ha), REZ (9981.98 ha), INZ (9542.37 ha), GOZ (6200.49 ha), DEZ (4333.06 ha), PSZ (3766.75 ha), AGZ (756.31 ha), and LRZ (462.59 ha), while PRZ accounted for the lowest area (244.64 ha). As shown in Fig. 5, UFZs such as COZ, HRZ, INZ, GOZ, and PSZ showed the highest impervious ratios (area of developed land to total area of UFZ) at > 60%, while AGZ, PRZ, and REZ showed the lowest impervious ratios (< 30%) but highest green ratios (> 60%).

In particular, most of the bare land in the study area was in DEZ, with a total area of 999.28 ha. Referring to the UFZ descriptions in Table 1, these bare lands in DEZ mainly comprised open spaces and demolition areas for urban construction, which would be developed into other types of urban land. Considering the acquisition timespan between the IKONOS (2012) and Landsat 8 images (2014–2015), the potential urban land cover transformation may induce a certain deviation in the analysis between DEZ and LST. Therefore, we decided to excluded the DEZ UFZs from subsequent analysis.

### LST details of UFZs

At pixel (Landsat 8, 30-m) scale (Fig. 3; Table 2), the LST varied significantly among different seasons, following an obvious decreasing trend from the warm to cold season. The highest LST in the study area was found on 19 August 2014, ranging from 21.67 to 46.28 °C, with a mean value of 35.30 °C. The lowest mean LST, however, was captured on 25 December 2014, at 3.75 °C. The LST variations also showed a similar trend, ranging from a largest standard deviation (SD) of 2.26 °C on 5 May 2014 to a smallest s.d. of 1.20 °C on 25 December 2014.

Significant differences in LST were revealed among different types of UFZ (Table 3). The “developed” UFZs, including INZ, COZ, GOZ, PSZ, and HRZ, had relative higher LST (> 20 °C) compared with the other UFZs during the warm seasons (May–October in 2014). Notably, the “ecological” UFZs (i.e., AGZ, PSZ, and REZ) showed higher LSTs than the “developed” UFZs in the cold seasons (December in 2014 to March in 2015) and more stable LST fluctuations (< 30 °C) across the whole year. The largest mean LST gap among these types of UFZs was 3.85 °C (2014/5/15), 3.59 °C (2014/8/19), 3.26 °C (2014/10/6), 1.72 °C (2014/12/25), and 2.55 °C (2015/3/15) in the study area.

**Table 2** Summary of land surface temperature (LST, °C) in the study area

Date acquisition time	Max. LST	Min. LST	Mean LST	S.D.
2014/05/15	41.16	16.69	29.46	2.26
2014/08/19	46.28	21.67	35.30	2.22
2014/10/06	35.45	3.98	22.47	2.01
2014/12/25	10.91	−8.96	3.75	1.20
2015/03/15	27.37	3.03	18.56	1.79

**Fig. 5** Land cover compositions of urban function zone (UFZ)

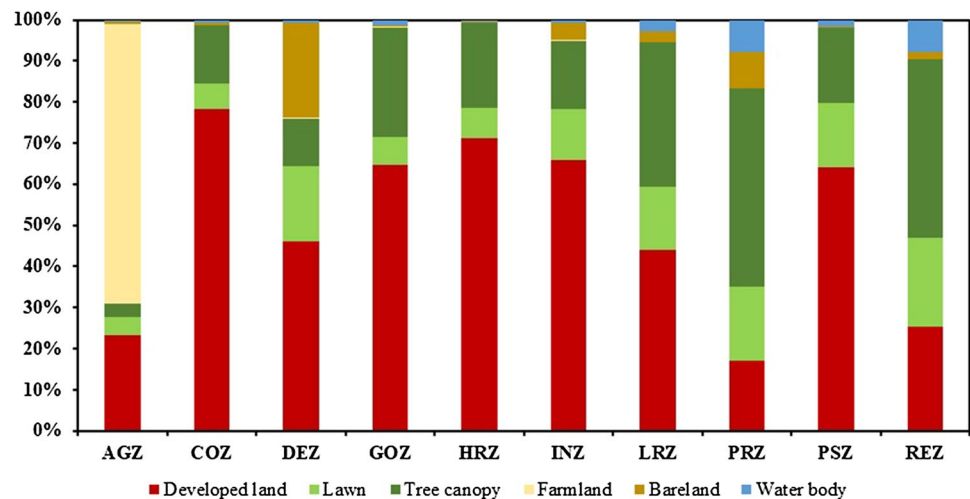


**Table 3** Summary of land surface temperature (LST, °C) of urban function zones

	2014/5/15	2014/8/19	2014/10/6	2014/12/25	2015/3/15
LRZ	28.57 <sup>CDE</sup>	34.39 <sup>CD</sup>	21.54 <sup>DE</sup>	3.62 <sup>C</sup>	18.29 <sup>CD</sup>
HRZ	29.53 <sup>BCD</sup>	35.62 <sup>B</sup>	22.43 <sup>BCD</sup>	3.42 <sup>C</sup>	17.96 <sup>D</sup>
GOZ	29.55 <sup>BC</sup>	35.83 <sup>AB</sup>	22.63 <sup>BCD</sup>	3.47 <sup>C</sup>	18.23 <sup>CD</sup>
INZ	31.44 <sup>A</sup>	36.83 <sup>A</sup>	24.20 <sup>A</sup>	4.41 <sup>B</sup>	19.73 <sup>AB</sup>
COZ	29.79 <sup>B</sup>	36.00 <sup>AB</sup>	22.85 <sup>B</sup>	3.45 <sup>C</sup>	18.03 <sup>D</sup>
REZ	28.33 <sup>CDE</sup>	33.96 <sup>D</sup>	21.63 <sup>CDE</sup>	3.96 <sup>BC</sup>	18.59 <sup>CD</sup>
PRZ	27.59 <sup>E</sup>	33.24 <sup>D</sup>	20.94 <sup>E</sup>	4.02 <sup>BC</sup>	19.14 <sup>BC</sup>
AGZ	29.23 <sup>BCD</sup>	33.54 <sup>D</sup>	21.66 <sup>CDE</sup>	5.14 <sup>A</sup>	20.51 <sup>A</sup>
PSZ	29.53 <sup>BCD</sup>	35.93 <sup>AB</sup>	22.77 <sup>BC</sup>	3.59 <sup>C</sup>	18.42 <sup>CD</sup>

HRZ high-density residential zone, LRZ low-density residential zone, GOZ government zone, INZ industry zone, COZ commercial zone, REZ recreational zone, PRZ preservation zone, AGZ agricultural zone, PSZ public service zone

Different letters indicate statistical difference at 0.05 level

The spatial clustering results showed that the LST of UFZs were significantly spatially autocorrelated, revealing obvious urban thermal agglomeration in the city. The Local Moran’s I analysis illustrating the spatial variations of LST hot/cold spots in different seasons is shown in Fig. 6. The hot spots, namely the HH clusters in Fig. 6, could be considered as regions with a significant UHI effect, whereas the cold spots (i.e., the LL clusters) as urban cold islands. The percentage areal coverage of HH clusters (versus the whole study area) was 17.62% (14 May 2014), 14.02% (19 August 2014), 15.02% (6 October 2014), 22.65% (25 December 2014), and 24.46% (15 March 2015), while that of LL clusters was 18.40%, 15.22%, 15.67%, 13.21%, and 15.00%, respectively. Spatially, the HH clusters showed a similar spatial distribution pattern, being mainly aggregated in the southern area. LL clusters tended to aggregate close to the north region of the study area, while some clusters of low values were also distributed in the central region. Especially on 15 March 2015, most of the clusters of low LST values tended to aggregate around the central region, as shown in Fig. 6. For all five LST images, the spatial outliers of LST high (low) values occupied a relatively small area and were scattered in the study area.

Figures 7 and 8 illustrate the UFZ compositions of HH and LL clusters in different seasons. During the warm season (from May to October in 2014), the HRZ, INZ, and COZ UFZs made the major contributions to the HH clusters. In the cold season (25 December 2014 and 15 March 2015), the REZ component increased significantly in the HH clusters. The UFZ compositions of the LL clusters were different from those of the HH clusters: REZ and HRZ were the main components of LL clusters, while the contribution of COZ increased significantly as the season changed from warm to cold.

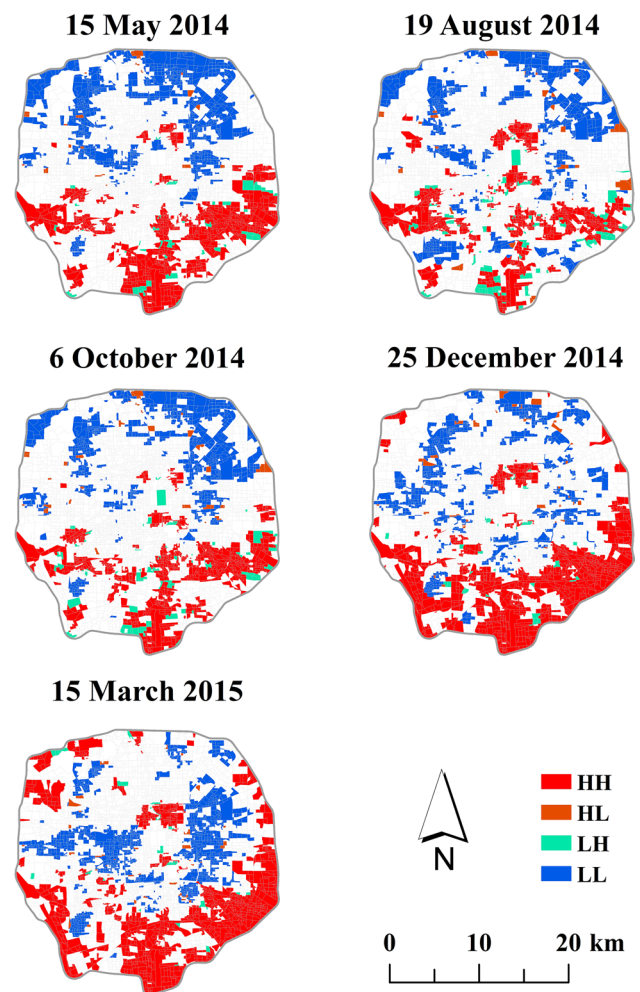


**Fig. 6** Spatial clusters of land surface temperatures (LSTs) of urban function zones using local Moran’s I. HH indicates that LSTs with high values aggregate, and LL indicates that LSTs with low values aggregate; a spatial outlier of LST high value is displayed in HL; a spatial outlier of low value is mapped in LH

Appendix Table 6 shows that more INZ, PSZ, and COZ UFZs tended to be in HH rather than LL clusters during the warm season, while more AGZ, REZ, PRZ, and LRZ UFZs tended to contribute to LL clusters. In the cold season, however, the ratios of the “ecological” UFZs such as AGZ, REZ, and PRZ increased in the HH clusters, while in contrast, “developed” UFZs such as HRZ, COZ, and GOZ tended to aggregate in LL clusters.

**Effects of the land cover composition on LST**

Table 4 presents the Pearson correlation coefficients between the largest LST variation (between 2014/8/19 and 2014/12/25) and the land cover composition of the study area. All land cover types were significantly related to the

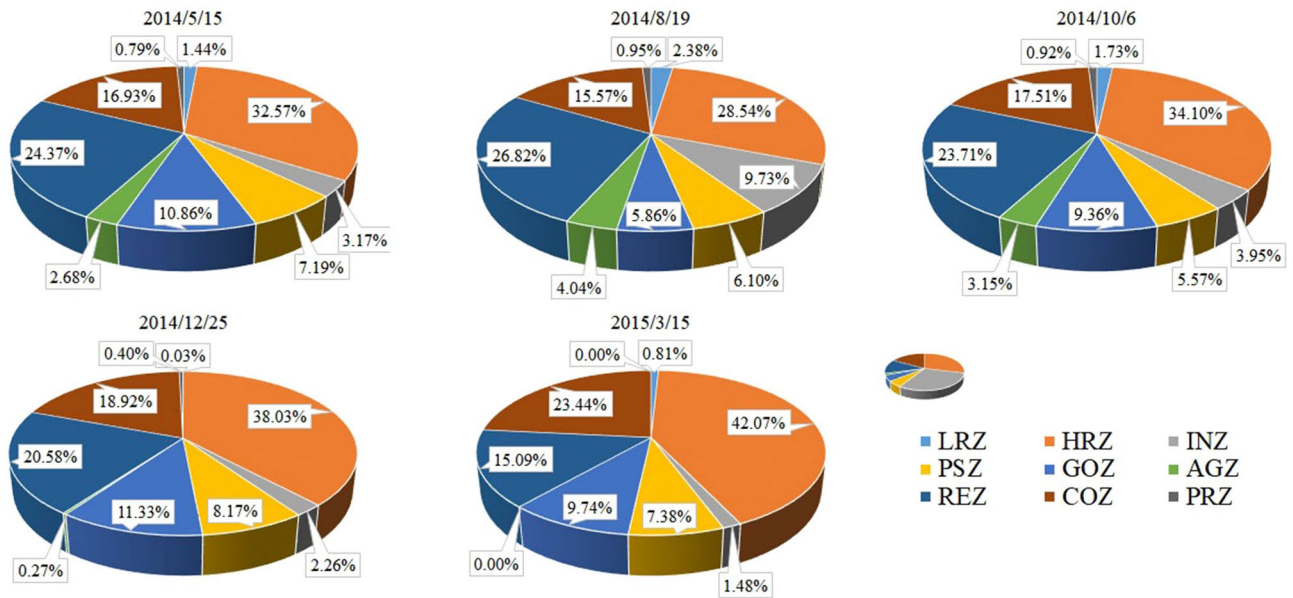


Fig. 7 The urban function zone compositions in HH clusters

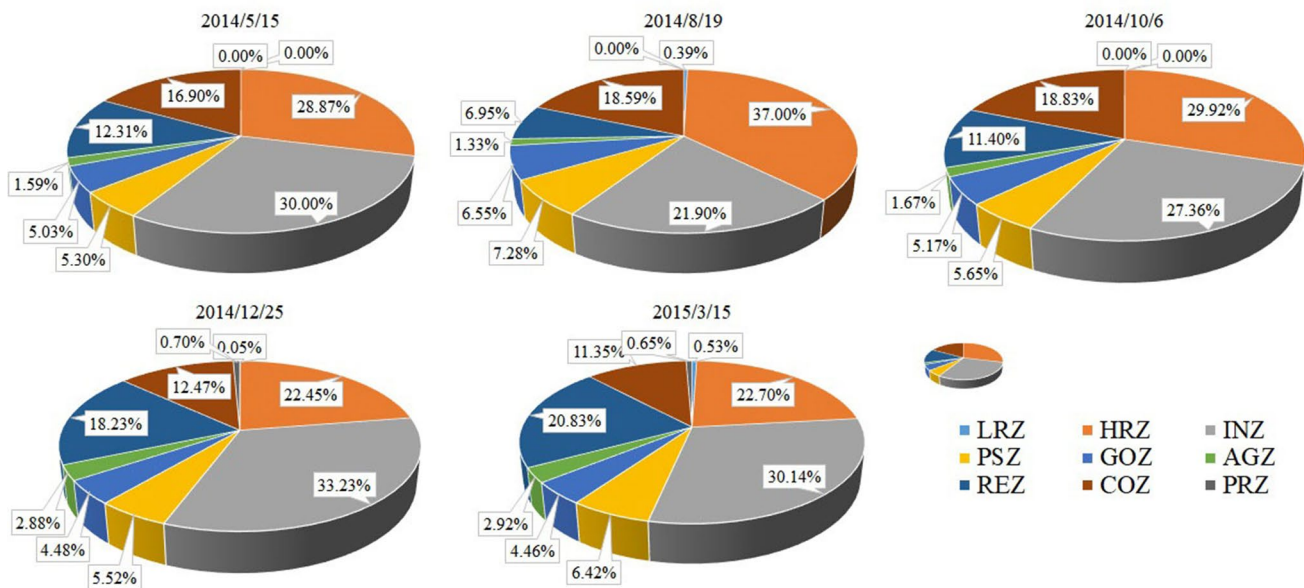


Fig. 8 The urban function zone compositions in LL clusters

LST variation. Among these, developed land showed the most significant and positive correlation with the LST variation, while forest showed the strongest negative correlation. These results indicate that the urban LST variation is mainly affected by developed land and green space.

The Pearson correlation coefficients between LSTs and land cover compositions in HH/LL clusters are reported in Table 5. Overall, urban developed land as well as forest were

found to show the strongest general relationship with LST. During the warm season, for both HH and LL clusters, a positive relationship between developed land and LST was found, while green land showed a negative relationship with LST. However, completely opposite correlation results were found between HH and LL clusters during the cold season. Specifically, as the temperature dropped, the correlation between developed/forest land and LST weakened (and even



**Table 4** Correlation coefficients between the variation (between 2014/8/19 and 2014/12/25) of land surface temperature (LST) and land cover composition (%) of urban function zones

Land cover composition	Bare land	Farmland	Forest	Grassland	Developed land
	-0.123**	-0.178**	-0.536**	-0.437**	0.739**

\*\*Correlation significant at 0.01 level (two-tailed)

lost significance) in the HH clusters, while the opposite correlation was found for both developed (opposite) and forest land (negative) in comparison with the warm season.

## Discussion

### Major factors affecting LST in different UFZs

This study explored the spatial patterns of LST assigned to different UFZs. Two different types of UFZ clusters were classified as “developed” and “ecological” UFZs. The “developed” UFZs (e.g., INZ, COZ, GOZ, PSZ, and HRZ) showed a similar, high LST variation among different seasons (with relatively higher LST in the hot season and lower LST in the cold season compared with “ecological” UFZs), while the “ecological” UFZs (i.e., AGZ, PSZ, and REZ) showed a similar, relatively stable LST variation. This indicates that these green urban zones functioned as effective air-conditioning areas, providing a warming effect in winter and a cooling effect in summer, thereby improving human comfort and the habitability of the city. This similarity among these two types of UFZ cluster can mainly be attributed to their similar landscape structure

(Sun and Chen 2017; Sun et al. 2013). The results presented in Table 4 show that developed land had the most significant effects on LST variations compared with other types of land cover. As shown in Fig. 5, the “developed” UFZs mainly consisted of impervious surfaces (e.g., concrete/metallic roofs, asphalt pavements, or brick squares) with a lower proportion of green space. These surfaces (termed urban grey surfaces; Tiwary and Kumar 2014) are characterized by lower albedo, latent heat flux, and thermal capacity (Morabito et al. 2016; Peng et al. 2016; Taha 1997), which will lead to more sensitive LST fluctuations compared with green spaces.

The correlation analysis revealed that the magnitudes of the LST were significantly correlated with the land cover composition of the UFZs, consistent with findings from previous studies (Kikegawa et al. 2006; Morabito et al. 2016; Zhou et al. 2011). Furthermore, the results of this study emphasize the changes in the relationship between the LST variations and the percentage of different types of land cover in different seasons. The results show that this correlation changed significantly for different types of clusters and seasons:

First, during the warm season, for both HH and LL clusters, the coverage of developed land of UFZs was the most important factor promoting LST, while the percentage cover of forest/grass land was the key factor mitigating LST. These effects can be explained by land surface characteristics such as albedo and evapotranspiration due to the percentage of developed and green land covers in the different UFZs (Amanollahi et al. 2016; Taha 1997). In addition, developed land is the main landscape type in INZ, COZ, GOZ, PSZ, and HRZ UFZs, which can be described by a concentration of anthropogenic activities within the urban area, leading to intensive energy use (e.g., for air conditioning and refrigeration systems, or waste heat produced by fossil fuels), all of which would promote UHI effects (Kikegawa et al. 2006; Zhou et al. 2011).

**Table 5** Correlation coefficients between land surface temperature and land cover composition (%) of HH/LL clusters

	Bare land	Farmland	Forest	Grassland	Developed land
<b>HH</b>					
2014/5/15	-0.071*	0.022	-0.524**	-0.237**	0.490**
2014/8/19	-0.142**	-0.099**	-0.516**	-0.444**	0.656**
2014/10/6	-0.122**	-0.049	-0.522**	-0.367**	0.588**
2014/12/25	0.040	0.056	-0.060	0.121**	-0.070*
2015/3/15	-0.029	0.134**	-0.057	0.015	0.017
<b>LL</b>					
2014/5/15	-0.007	-0.126**	-0.402**	-0.194**	0.518**
2014/8/19	-0.002	-0.169**	-0.436**	-0.227**	0.567**
2014/10/6	-0.049	-0.065	-0.249**	-0.194**	0.346**
2014/12/25	-0.014	0.099**	0.217**	0.070*	-0.214**
2015/3/15	-0.024	-	0.189**	-0.006	-0.114**

\*Correlation significant at 0.05 level (two-tailed)

\*\*Correlation significant at 0.01 level (two-tailed)

Second, in comparison with the warm season, the role of each land cover in affecting the LST altered during the cold season. The relation between most types of land cover and the LST lost its significance in the HH clusters, whereas for the LL clusters, the role of developed land and forest in affecting the LST was interchanged in comparison with the warm season. This result is consistent with findings by Haashemi et al. (2016), which may be largely due to the difference in the UFZ composition between HH and LL clusters. These results show that more “developed” UFZs were attributed to LL clusters while more “ecological” UFZs were attributed to HH clusters, along with the temperature drops (Appendix Table 6). The main forest types in LL clusters were recorded as deciduous vegetation, such as *Populus tomentosa*, *Salix babylonica*, and *Sophora japonica* (Meng et al. 2004). The low leaf area of deciduous trees as well as the cold climate would greatly lessen canopy evapotranspiration due to latent heat exchange. In addition, compared with developed land, the water content of plants retains more heat against cold and freezing. The capacity of forest to mitigate LST would thus be reduced (Haashemi et al. 2016; Zhou et al. 2014).

### Urban management implications

Some implications of these results may be useful for current and future urban planning. First, the local indicator of spatial association (LISA) maps present the fine-scale spatial distribution of LST clusters, revealing various urban thermal concentrations in different seasons (Fig. 6). The LST hot spots (HH clusters) were mainly distributed in the areas surrounding the city rather than the central location, in clear distinction to the LST cold spots (LL clusters). This may provide reference targets for decision-makers in developing specific strategies to moderate urban thermal environments. Second, the urban thermal characteristics were found to be closely related to the UFZ type. UFZs such as INZ, COZ, GOZ, PSZ, and HRZ showed relatively high thermal sensitivity and were more likely to be potential hot spots of the UHI effect compared with UFZs such as AGZ, PSZ, and REZ. According to Sun et al. (2013), reasonable landscape planning is needed to rearrange the spatial configuration of different types of UFZs within a city. Increasing the landscape connectivity between these UFZs and vegetation/water corridors/patches is helpful for improving heat exchange and thus the urban thermal environment (Gago et al. 2013; Sun and Chen 2012). Finally, the spatial differences in LST were mainly caused by the various landscape compositions in the different types of UFZ. The results of this study reveal that the composition of impervious (i.e., developed) and preservation (i.e., forest) areas are two key landscape indicators

regarding the UHI effect. In addition, these two kinds of land cover show different thermal inertia characteristics in different seasons. This may help urban regulators to modulate landscape compositions rationally to mitigate the UHI phenomenon in different types of UFZ.

### Limitations of this study

This study has its limitations. First, this study used UFZs as the basic spatial units for the urban LST analysis. The use of UFZs is based on the assumption that urban streets/rivers act as physical barriers to thermal exchange between different urban blocks (Sun et al. 2013; Yao et al. 2015). Besides UFZs, spatial units such as image pixels (Haashemi et al. 2016), a regular grid (Chen et al. 2014), concentric circles (Majumdar and Biswas 2016), or other landscape units, e.g., HERCULES by Zhou et al. (2011), have also been applied for UHI analysis. This may lead to uncertainty in data analysis, because there is still no definitive spatial unit for UHI research. Second, this study quantified the significant relationship between land cover compositions and LST in UFZs. Beyond that, it has been reported that the configuration of land cover is also significantly correlated with LST (Chen et al. 2014; Peng et al. 2016; Zhou et al. 2011), making it desirable to quantify the effect of urban landscape characteristics on the UHI effect more accurately in future work. Finally, the land surface temperature was used to represent the thermal heterogeneity of the study area, which is different from the air temperature (Sun et al. 2013). Greater effort is needed to refine urban thermal research by using more different types of climate data.

### Conclusions

This study attempted to expand understanding of the UHI effect from the perspective of UFZs and landscape structure. The main results can be summarized as followed:

1. The LST presented obvious spatiotemporal heterogeneity across different UFZs and seasons. Urban residential, industrial, and commercial zones contributed most of the UHI regions during the warm season. Besides, part of the urban recreation zone functioned as a UHI region during the cold season.
2. The urban thermal heterogeneity was strongly affected by both urban developed and green land. However, their thermal contributions varied in different seasons, with urban green spaces presenting an effective air-condition-

ing function and benefiting the urban thermal environment.

Generally, the urban thermal environment showed significant complexity due to the diversity of the urban functions and landscape structure in the studied region. This study expands understanding on the relationship between urban functions, landscape, and urban thermal environment, and thus could have scientific implications for future urban landscape planning to mitigate the UHI phenomenon.

**Acknowledgements** We sincerely thank the editors and two anonymous reviewers for their valuable advice regarding revision of this manuscript. This work was financed by the Natural Science Foundation of China (41701206), the Natural Science Foundation of Shandong Province (ZR2017BD011), and the China Postdoctoral Science Foundation (2017M622256).

## Appendix

See Table 6.

**Table 6** Characteristics of urban function zones (UFZs) in clusters of high and low values (i.e., HH and LL) identified by local Moran's I. Percentage (%) values indicate the ratio between the area of each UFZ in HH (or LL) clusters and the total area of the UFZ

HH			LL		
UFZ	Area (ha)	Percentage (%)	UFZ	Area (ha)	Percentage (%)
2014/5/15					
HRZ	3394.73	15.97	LRZ	177.36	38.34
INZ	3527.03	36.96	HRZ	3998.43	18.81
PSZ	622.64	16.53	INZ	389.38	4.08
GOZ	591.80	9.54	PSZ	882.24	23.42
AGZ	187.12	24.74	GOZ	1332.83	21.50
REZ	1447.81	14.50	AGZ	329.39	43.55
COZ	1986.64	19.50	REZ	2991.51	29.97
			COZ	2078.93	20.40
			PRZ	96.41	39.41
2014/8/19					
LRZ	36.37	7.86	LRZ	242.13	52.34
HRZ	3461.14	16.28	HRZ	2899.13	13.64
INZ	2048.66	21.47	INZ	988.92	10.36
PSZ	680.61	18.07	PSZ	619.37	16.44
GOZ	613.05	9.89	GOZ	595.13	9.60
AGZ	124.46	16.46	AGZ	410.91	54.33
REZ	650.16	6.51	REZ	2724.94	27.30
COZ	1738.883	17.07	COZ	1581.59	15.52
			PRZ	96.41	39.41

**Table 6** (continued)

HH			LL		
UFZ	Area (ha)	Percentage (%)	UFZ	Area (ha)	Percentage (%)
2014/10/6					
HRZ	2999.44	14.11	LRZ	180.62	39.05
INZ	2743.13	28.75	HRZ	3565.42	16.77
PSZ	566.53	15.04	INZ	413.13	4.33
GOZ	518.79	8.37	PSZ	581.92	15.45
AGZ	167.37	22.13	GOZ	978.73	15.78
REZ	1143.04	11.45	AGZ	329.39	43.55
COZ	1888.17	18.53	REZ	2479.44	24.84
			COZ	1830.22	17.96
			PRZ	96.41	39.41
2014/12/25					
LRZ	7.57	1.64	LRZ	2.81	0.61
HRZ	3392.14	15.96	HRZ	3352.30	15.77
INZ	5021.46	52.62	INZ	199.48	2.09
PSZ	833.78	22.14	PSZ	720.09	19.12
GOZ	677.46	10.93	GOZ	998.24	16.10
AGZ	434.49	57.45	AGZ	23.60	3.12
REZ	2755.13	27.60	REZ	1813.90	18.17
COZ	1884.10	18.49	COZ	1668.02	16.37
PRZ	105.64	43.18	PRZ	35.68	14.58
2015/3/15					
LRZ	86.69	18.74	LRZ	81.12	17.54
HRZ	3705.23	17.43	HRZ	4211.48	19.81
INZ	4920.45	51.56	INZ	147.68	1.54
PSZ	1047.67	27.81	PSZ	738.43	19.60
GOZ	728.53	11.75	GOZ	975.27	15.73
AGZ	476.38	62.99	REZ	1510.33	15.13
REZ	3400.78	34.07	COZ	2347.12	23.03
COZ	1852.41	18.18			
PRZ	105.64	43.18			

## References

Almusaed A (2011) Biophilic and bioclimatic architecture: analytical therapy for the next generation of passive sustainable architecture. *Harvard J Asiatic Stud* 38:5–34

Amanollahi J, Tzani C, Ramli MF, Abdullah AM (2016) Urban heat evolution in a tropical area utilizing Landsat imagery. *Atmos Res* 167:175–182

Anselin L (1995) Local Indicators of Spatial Association—LISA. *Geogr Anal* 27:93–115

Arnfield AJ (2003) Two decades of urban climate research: a review of turbulence, exchanges of energy and water, and the urban heat island. *Int J Climatol* 23:1–26

Beijing Statistical Bureau (2012) Beijing statistical yearbook. Beijing Statistical Bureau. China Statistics Press, Beijing

Cao X, Onishi A, Chen J, Imura H (2010) Quantifying the cool island intensity of urban parks using ASTER and IKONOS data. *Landscape Urban Plan* 96:224–231

- Carlson TN, Traci Arthur S (2000) The impact of land use—land cover changes due to urbanization on surface microclimate and hydrology: a satellite perspective. *Glob Planet Change* 25:49–65
- Chen A, Yao L, Sun R, Chen L (2014) How many metrics are required to identify the effects of the landscape pattern on land surface temperature? *Ecol Ind* 45:424–433
- Chen A, Zhao X, Yao L, Chen L (2016) Application of a new integrated landscape index to predict potential urban heat islands. *Ecol Indic* 69:828–835
- Dos Santos AR, de Oliveira FS, da Silva AG, Gleriani JM, Gonçalves W, Moreira GL, Silva FG, Branco ERF, Moura MM, da Silva RG, Juvanhof RS, de Souza KB, Ribeiro CAAS, de Queiroz VT, Costa AV, Lorenzon AS, Domingues GF, Marcatti GE, de Castro NLM, Resende RT, Gonzales DE, de Almeida Telles LA, Teixeira TR, dos Santos GMADA, Mota PHS (2017) Spatial and temporal distribution of urban heat islands. *Sci Total Environ* 605:946–956
- Gago EJ, Roldan J, Pacheco-Torres R, Ordóñez J (2013) The city and urban heat islands: a review of strategies to mitigate adverse effects. *Renew Sustain Energy Rev* 25:749–758
- Haashemi S, Weng Q, Darvishi A, Alavipanah SK (2016) Seasonal variations of the surface urban heat island in a semi-arid city. *Remote Sens* 8(4):352
- Kardinal Jusuf S, Wong NH, Hagen E, Anggoro R, Hong Y (2007) The influence of land use on the urban heat island in Singapore. *Habitat Int* 31:232–242
- Kikegawa Y, Genchi Y, Kondo H, Hanaki K (2006) Impacts of city-block-scale countermeasures against urban heat-island phenomena upon a building's energy-consumption for air-conditioning. *Appl Energy* 83:649–668
- Li J, Song C, Cao L, Zhu F, Meng X, Wu J (2011) Impacts of landscape structure on surface urban heat islands: a case study of Shanghai, China. *Remote Sens Environ* 115:3249–3263
- Ma Y, Kuang Y, Huang N (2010) Coupling urbanization analyses for studying urban thermal environment and its interplay with biophysical parameters based on TM/ETM + imagery. *Int J Appl Earth Obs Geoinf* 12:110–118
- Majumdar DD, Biswas A (2016) Quantifying land surface temperature change from LISA clusters: an alternative approach to identifying urban land use transformation. *Landsc Urban Plan* 153:51–65
- Meng Q (2016) The spatiotemporal characteristics of environmental hazards caused by offshore oil and gas operations in the Gulf of Mexico. *Sci Total Environ* 565:663
- Meng X, Ouyang Z, Cui G, Li W, Zheng H (2004) Composition of plant species and their distribution patterns in Beijing urban ecosystem. *Acta Ecol Sin* 24:2200–2206
- Mitchell A (1999) *The ESRI guide to GIS analysis*. ESRI Press
- Morabito M, Crisci A, Messeri A, Orlandini S, Raschi A, Maracchi G, Munafò M (2016) The impact of built-up surfaces on land surface temperatures in Italian urban areas. *Sci Total Environ* 551–552:317–326
- Peng J, Xie P, Liu Y, Ma J (2016) Urban thermal environment dynamics and associated landscape pattern factors: a case study in the Beijing metropolitan region. *Remote Sens Environ* 173:145–155
- Sun R, Chen L (2012) How can urban water bodies be designed for climate adaptation? *Landsc Urban Plan* 105:27–33
- Sun R, Chen L (2017) Effects of green space dynamics on urban heat islands: mitigation and diversification. *Ecosyst Serv* 23:38–46
- Sun R, Lü Y, Chen L, Yang L, Chen A (2013) Assessing the stability of annual temperatures for different urban functional zones. *Build Environ* 65:90–98
- Taha H (1997) Urban climates and heat islands: albedo, evapotranspiration, and anthropogenic heat. *Energy Build* 25:99–103
- Tian GJ, Wu JG, Yang ZF (2010) Spatial pattern of urban functions in the Beijing metropolitan region. *Habitat Int* 34:249–255
- Tiwary A, Kumar P (2014) Impact evaluation of green–grey infrastructure interaction on built-space integrity: an emerging perspective to urban ecosystem service. *Sci Total Environ* 487:350–360
- Vos PEJ, Maiheu B, Vankerkom J, Janssen S (2013) Improving local air quality in cities: to tree or not to tree? *Environ Pollut* 183:113–122
- Weng Q (2009) Thermal infrared remote sensing for urban climate and environmental studies: methods, applications, and trends. *ISPRS J Photogram Remote Sens* 64:335–344
- Yang Y, Shang S, Jiang L (2012) Remote sensing temporal and spatial patterns of evapotranspiration and the responses to water management in a large irrigation district of North China. *Agric For Meteorol* 164:112–122
- Yao L, Chen L, Wei W, Sun R (2015) Potential reduction in urban runoff by green spaces in Beijing: a scenario analysis. *Urban For Urban Green* 14:300–308
- Zhou W, Cadenasso ML (2012) Effects of patch characteristics and within patch heterogeneity on the accuracy of urban land cover estimates from visual interpretation. *Landsc Ecol* 27:1291–1305
- Zhou W, Huang G, Cadenasso ML (2011) Does spatial configuration matter? Understanding the effects of land cover pattern on land surface temperature in urban landscapes. *Landsc Urban Plan* 102:54–63
- Zhou W, Qian Y, Li X, Li W, Han L (2014) Relationships between land cover and the surface urban heat island: seasonal variability and effects of spatial and thematic resolution of land cover data on predicting land surface temperatures. *Landsc Ecol* 29:153–167